AD-A105 233 SAN JOSE STATE UNIV CA SCHOOL OF ENGINEERING F/G 20/2
DEEP LEVELS IN ALX GA(1-X) AS:FE SINGLE CRYSTALS.(U)
MAR 81 R A RAO AFOSR-80-0099
UNCLASSIFIED TR-81-01 AFOSR-TR-81-0696 NL

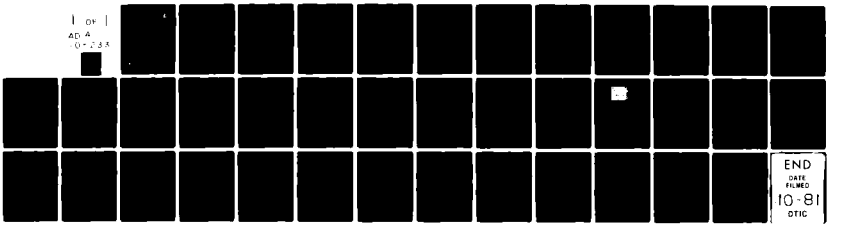

SCHOOL OF ENGINEERING

SAN JOSE STATE UNIVERSITY
SAN JOSE, CA. 95192

DEEP LEVELS IN $Al_x Ga_{1-x} As$: Fe SINGLE CRYSTALS

by

Dr. Rangaiya A. Rao

March 1, 1981

Technical Report No. 81-01

Prepared under
Air Force Office of Scientific Research
Grant AFOSR 80-0099

SECURITY CLASSIFICATION OF THIS PAGE (When Data Entered)

REPORT DOCUMENTATION PAGE	READ INSTRUCTIONS BEFORE COMPLETING FORM
1. REPORT NUMBER: AFOSR-TR-81-0696	2. GOVT ACCESSION NO.: AD-A105233	3. RECIPIENT'S CATALOG NUMBER
4. TITLE (and Subtitle): "DEEP LEVELS IN $Al_x Ga_{1-x} AS$:Fe SINGLE CRYSTALS c	5. TYPE OF REPORT & PERIOD COVERED: Interim rpt. 1 March 1981
	6. PERFORMING ORG. REPORT NUMBER
7. AUTHOR(s): R A Rao	8. CONTRACT OR GRANT NUMBER(s): AFOSR-80-0099
9. PERFORMING ORGANIZATION NAME AND ADDRESS: San Jose State University, San Jose, CA 95192	10. PROGRAM ELEMENT, PROJECT, TASK AREA & WORK UNIT NUMBERS: 2306/D9, 61102F
11. CONTROLLING OFFICE NAME AND ADDRESS: Air Force Office of Scientific Research/NE, Bolling AFB, DC 20332	12. REPORT DATE: 1 March 1981; 13. NUMBER OF PAGES: 36
14. MONITORING AGENCY NAME & ADDRESS (if different from Controlling Office)	15. SECURITY CLASS. (of this report): UNCLASSIFIED; 15a. DECLASSIFICATION DOWNGRADING SCHEDULE

16. DISTRIBUTION STATEMENT (of this Report)

Approved for public release; distribution unlimited

TR-81-0696

17. DISTRIBUTION STATEMENT (of the abstract entered in Block 20, if different from Report)

18. SUPPLEMENTARY NOTES

19. KEY WORDS (Continue on reverse side if necessary and identify by block number)

20. ABSTRACT (Continue on reverse side if necessary and identify by block number)

Deep levels in $Al_x Ga_{1-x}As$:Fe were investigated using deep level transient spectroscopy (DLTS) and deep level photoluminescence measurements. In the DLTS experiments, p-$Al_xGa_{1-x}As$:Fe/n^+-GaAs:Te heterojunctions were used. The aluminum compositions in the p-$Al_xGa_{1-x}As$ layers were 0.39, 0.56, and 0.71. In the smaple 626x-2, with aluminum composition x=0.39, four hole traps at 0.012 eV, 0.22 eV, 0.48 eV, and 0.6eV were detected. In the sample 526x-2, with x=0.56, two hole traps with activation energies 0.46 eV and 0.49 eV

DD FORM 1 JAN 73 1473 EDITION OF 1 NOV 65 IS OBSOLETE

UNCLASSIFIED 412578

SECURITY CLASSIFICATION OF THIS PAGE (When Data Entered)

were detected. In the sample 706x-1, with x=0.71, two hole traps at 0.28 eV and 0.75 eV above the valence band edge were detected. In addition, an electron trap at 0.154 eV below the conduction band was also detected in that smaple. The defect densities were in the range $4X10^{13}cm^{-3}$ to $5X10^{15}$ cm^{-3} and the capture cross-sections ranged from $3X10^{-21}$ cm^2 to $7X10^{-10}cm^2$. The hole traps at 0.48 eV and 0.6 eV in smaple 626x-2, at 0.46 eV and 0.49 eV in smaple 526x-2, and at 0.75 eV in smaple 706x-1 may be due tocopper or the so-called "level A" reported by Lang, Logan and Kimmerling. The 0.9 eV hole trap seen in some 626x-2 smaples is probably due to Fe. Photoluminescence measurements made on p-$Al_xGa_{1-x}As$/GaAs:Cr layers with x=0.06, 0.12, 0.24, and 0.31 showed a sharp peak at 0.37 eV. This emission is probably due to the internal d-d transitions of Fe^{2+} in the GaAs substrate. In a sample grown on GaAs:Te substrate, a broad peak at 1.23 eV was observed. This peak corresponds to the emission due to the Te donor- Ga vacancy complex in GaAs. Several suggestions for future work are made.

DEEP LEVELS IN $Al_xGa_{1-x}As$:Fe SINGLE CRYSTALS

by

Dr. Rangaiya A. Rao

March 1, 1981

Technical Report No. 81-01

Prepared under

Air Force Office of Scientific Research
Grant *AFOSR 80-0099*

School of Engineering
San Jose State University San Jose, California

ABSTRACT

Deep levels in $Al_xGa_{1-x}As$:Fe were investigated using deep level transient spectroscopy (DLTS) and deep level photoluminescence measurements. In the DLTS experiments, p-$Al_xGa_{1-x}As$:Fe/n^+-GaAs:Te heterojunctions were used. The aluminum compositions in the p-$Al_xGa_{1-x}As$ layers were 0.39, 0.56, and 0.71. In the sample 626x-2, with aluminum composition x=0.39, four hole traps at 0.012 eV, 0.22 eV, 0.48 eV, and 0.6 eV were detected. In the sample 526x-2, with x=0.56, two hole traps with activation energies 0.46 eV and 0.49 eV were detected. In the sample 706x-1, with x=0.71, two hole traps at 0.28 eV and 0.75 eV above the valence band edge were detected. In addition, an electron trap at 0.154 eV below the conduction band was also detected in that sample. The defect densities were in the range $4x10^{13}$ cm^{-3} to $5x10^{15}$ cm^{-3} and the capture cross-sections ranged from $3x10^{-21}$ cm^2 to $7x10^{-10}$ cm^2. The hole traps at 0.48 eV and 0.6 eV in sample 626x-2, at 0.46 eV and 0.49 eV in sample 526x-2, and at 0.75 eV in sample 706x-1 may be due to copper or the so-called 'level A' reported by Lang, Logan and Kimmerling. The 0.9 eV hole trap seen in some 626x-2 samples is probably due to Fe.

Photoluminescence measurements made on p-$Al_xGa_{1-x}As$/GaAs:Cr layers with x=0.06, 0.12, 0.24, and 0.31 showed a sharp peak at 0.37 eV. This emission is probably due to the internal d-d transitions of Fe^{2+} in the GaAs substrate. In a sample grown on GaAs:Te substrate, a broad peak at 1.23 eV was observed. This peak corresponds to the emission due to the Te donor- Ga vacancy complex in GaAs. Several suggestions for future work are made.

ACKNOWLEDGMENTS

I wish to acknowledge with deep gratitude the help and encouragement I received from Dr. Millard Meir, Dr. Phil Won Yu, Dietrich W. Langer, and Dr. Cole Litton of the Avionics Laboratory at the Wright-Patterson Air Force Base, Ohio in performing the experiments. I wish to thank the scientists in the Avionics Laboratory for the stimulating discussions.

I am grateful to Prof. Gerald Pearson of Stanford University for his help in growing the crystals and to Profs. Evan Moustakas and Dean Pinson of San Jose State University for their encouragement.

This work was supported by a mini grant AFOSR 80-0099 from the Air Force Office of Scientific Research.

Chapter 1

1.1 Introduction

Deep levels are energy levels in the bandgap of a semiconductor with activation energies which are large compared to kT. At a deep defect, the carrier wavefunction is localized near the site of the defect and, hence, delocalized in k-space. The defect can couple to a variety of phonons and interacts strongly with the lattice. Deep states generally tend to be nonradiative centers. Physically, they could result from certain chemical impurities, native defects such as vacancies, complexes involving native defects and impurities, surfaces, and interfaces. A variety of deep centers are almost always present in semiconductor crystals. They may be introduced intentionally into a semiconductor crystal by various methods. Gold introduces a deep acceptor level and a deep donor level in silicon. Gold may be evaporated onto the surface of a silicon wafer and then diffused-in by heating the wafer at a temperature of the order of 900 C for several minutes so that the gold atoms distribute themselves uniformly in the silicon crystal. Impurities like chromium and iron may be added to the melt from which GaAs, $Al_xGa_{1-x}As$, and other semiconductors are grown by liquid phase epitaxy. Heat treatment and bombardment by energetic electrons also create deep centers in semiconductors. Deep levels affect device performance in many ways. Device gain and speed are functions of carrier lifetime, carrier compensation, and carrier mobility, all of which are related to the presence of deep defects. The emission wavelength and the efficiency of light-emitting diodes and semiconductor lasers are affected by deep levels. Degradation and failure of $Al_xGa_{1-x}As$ heterojunction lasers may be often traced to nonradiative centers with energy levels deep in the bandgap. Deep

centers may be studied by a variety of experimental methods -- thermally stimulated capacitance [1], thermally stimulated current [2], photo capacitance [3], transient capacitance [4], deep level transient spectroscopy (DLTS) [5], and deep level photoluminescence. In this study we will be mostly concerned with deep level transient spectroscopy of centers in p-$Al_xGa_{1-x}As$/ n^+-GaAs heterojunctions.

1.2 Capture and Emission Processes in Deep Traps

It is useful to distinguish between a trap and a recombination center. A trap has a large capture rate for one type of carrier (electron or hole) while a recombination center has a large capture rate for both types of carrier. Hence, it is more appropriate to talk about the capture cross-section σ, of a center for a particular type of carrier. The capture rate for holes by traps in a region of semiconductor is given by:

$$c_p = \sigma_p \langle v_p \rangle p \qquad (1)$$

where c_p = Capture rate for holes (sec^{-1})

σ_p = Capture cross-section for holes (cm^2)

$\langle v_p \rangle$ = Average thermal velocity of holes (cm/sec)

p = Hole concentration (cm^{-3})

A similar equation holds for electrons:

$$c_n = \sigma_n \langle v_n \rangle n \qquad (2)$$

In our notation, exchange (by the center) of carriers with the valence band is referred to as 'hole capture' or 'hole emission' while exchange of carriers with the conduction band is called 'electron capture' or 'electron emission'. In the depletion region of a reverse biased p-n junction, carrier concentrations are negligible. In such a depletion region, if a center which is located in the lower part of the bandgap captures a hole, it is more likely to emit it back to the valence band before it can capture an electron and complete the recombination process. Such a center is called a hole trap. The emission rate is a function of the temperature and the depth of the trap from the band edge. In particular, for hole emission:

$$e_p = \frac{\sigma_p < v_p > N_v}{g} \exp(-\Delta E/kT) \qquad (3)$$

where the thermal velocity of a hole, $< v_p >$, and the effective density of states, N_v are given by

$$< v_p > = \sqrt{\frac{3kT}{m_h^*}} \quad \text{and} \qquad (4)$$

$$N_v = (2/h^3)(2\pi m_h^* kT)^{3/2} \qquad (5)$$

In the above equations,

ΔE = depth of the hole trap from the valence band edge

g = The degeneracy of the state

m_h^* = Effective mass of holes

k = Boltzmann Constant

h = Planck's Constant

A similar equation holds for the emission rate of electrons into the conduction band.

1.3 The Rate Equation

The electron population in the trap increases by the capture of an electron (c_n) and also by the emission of a hole (e_p) as illustrated in Fig. 1. Similarly, the electron population in the trap decreases by the capture

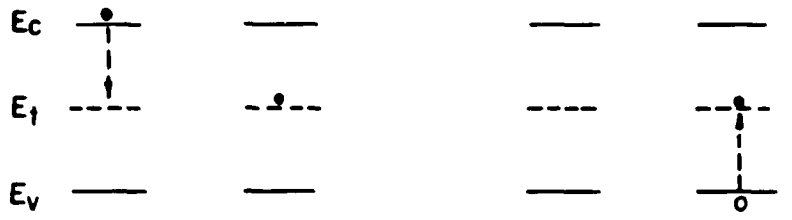

FIG. 1: ILLUSTRATION OF ELECTRON CAPTURE AND HOLE EMISSION

of a hole (c_p) and also by the emission of an electron (e_n). The rate at which electrons enter the trap is proportional to the number of empty traps and the rate at which electrons leave the trap is proportional to the number of filled (by electrons) traps. The net rate of change in the electron population of traps is given by the rate equation:

$$\frac{dN(t)}{dt} = (c_n + e_p)\,(N_T - N(t)) - (c_p + e_n)\,N(t) \qquad (6)$$

where

N_T = Total number of traps

$N(t)$ = Number of traps filled (by electrons) at time t

In the case of a hole trap in the depletion region of an n+-p junction, hole emission dominates, i.e., c_n, c_p, and $e_n \to 0$. With the traps filled with holes (or empty of electrons) at t=0, we have $N(t)=0$ for $t \leq 0$. The solution for the rate equation is:

$$N(t) = N_T(1-e^{-e_p t}) \text{ for } t \geq 0 \qquad (7)$$

1.4 Capacitance Transient

Capacitance transient measurements provide a powerful method for studying deep levels. A p-n junction (or a Schottky barrier) diode is made of the semiconductor material to be studied. N-type semiconductors are generally suitable for Schottky barriers, and in the case of a p-type semiconductor, an n+-p junction is used. The traps in the depletion region of a reverse-biased p-n junction are induced to capture carriers by applying a suitable voltage pulse of a short duration. When the pulse is removed, the captured carriers are re-emitted to the bands and the capacitance of the junction relaxes back to its quiescent value with a time constant equal to the time constant of the emission process as illustrated in Figs. 2, 3, and 4.

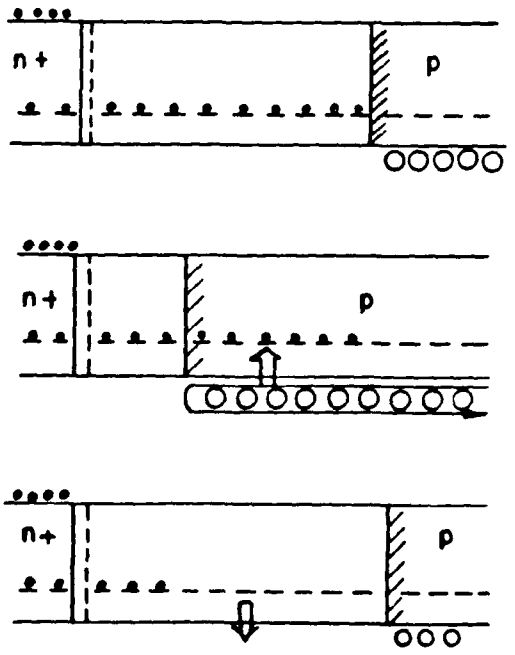

Fig. 2: Illustration of the capacitance transient method.

As an example, we consider an n+-p junction and we wish to study the hole traps in the p-region. Under reverse bias, the depletion region is wide and is almost entirely located on the p-side of the metallurgical junction. In this discussion, we shall assume acceptor-like traps in the lower half of the bandgap so that a trap is neutral when empty of electrons and negatively charged and ready to capture a hole when filled with electrons. Let us look at the hole traps in the p-region. In the quiescent reverse-biased condition, the hole traps in the depletion region are filled with electrons. The net charge density

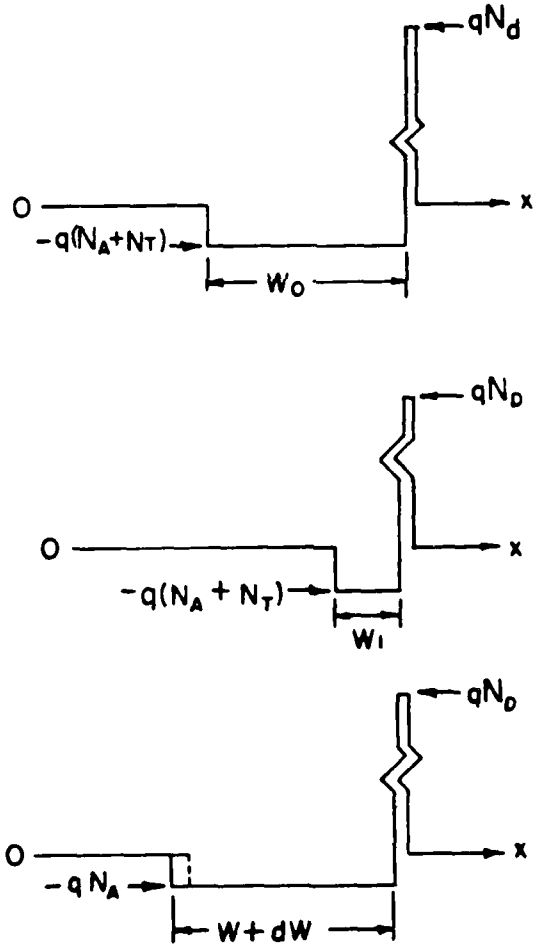

Fig. 3: Net charge density and depletion layer width before, during and after the majority carrier pulse.

on the p-side of the depletion region is $-q(N_A + N_T)$ where N_A is the concentration of ionized acceptors and N_T is the concentration of negatively charged hole traps. The depletion region width is W_o and the junction capacitance is C_o. A pulse of short duration (called the majority carrier pulse) which brings the p-n junction to the zero-biased condition reduces the depletion region width to W_1 and the capacitance increases to C_1. During this period of time, majority carrier holes are

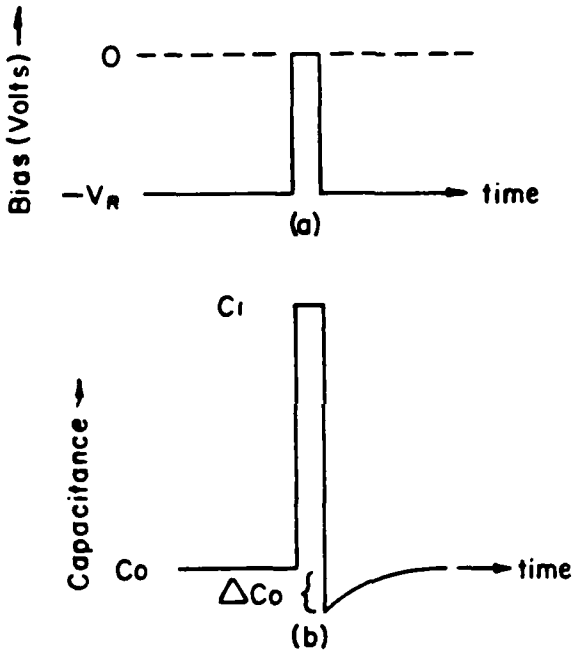

Fig. 4: a) Bias versus time b) Capacitance versus time

brought in to fill the traps with holes (i.e., to empty them of electrons). Immediately after the removal of the majority carrier pulse, the traps are empty of electrons and the net charge density is reduced to $-qN_A$. The system responds immediately to this change in net charge density by removing holes from a small region ΔW near the edge of the depletion region so that the depletion region widens to $W_o + \Delta W$. The capacitance drops to $C_o - \Delta C_o$. During the transient, the traps in

the depletion region emit holes to the valence band at an emission rate characteristic of the temperature and the location of the trap in the band gap. The emitted holes are in a region of large electric field and are swept away from the depletion region by the electric field. As the holes are released from the traps and swept away, the capacitance rises from $C_o - \Delta C_o$ to C_o with a time constant equal to the emission time constant of holes from the traps.

In practice, the height and duration of the majority carrier pulse are made large enough so that the traps in the depletion region are completely filled with holes (emptied of electrons) during this pulse. Under these conditions:

$$N_T = 2 N_A \Delta C_o / C_o \qquad (8)$$

where N_A is the net acceptor concentration on the p-side. The concentration of the majority carrier traps can be calculated from Eq. (8). In Eq. (3), the exponential term dominates the temperature dependence of the emission rate. The 'prefactor', $\sigma_p \langle v_p \rangle N_v/g$, is a mild function of temperature. Hence a plot of ln e_p versus $1/kT$ is a straight line with a slope, $-\Delta E$. The time constant τ of the capacitance transient is equal to the reciprocal of the emission rate, e_p. The experiment is repeated at several temperatures and a plot of ln $1/\tau$ versus $1/kT$ is obtained. The slope of this straight line gives the activation energy ΔE.

1.5 Deep Level Transient Spectroscopy (DLTS)

In deep level transient spectroscopy, an emission 'rate window' may be set so that the measuring system will respond only to transients with

emission rates which lie within that window. The emission rate of a trap is a function of temperature, and hence, if we slowly vary the temperature of the sample, the emission rate of the traps falls within the rate window only at a particular temperature and a signal peak is obtained at that temperature. If the rate window is changed to a new value and the thermal scan is repeated, the DLTS peak appears at a different temperature. Thus, a plot of ln (emission rate window) versus 1/T (where T is the temperature at which the DLTS peak appears for a particular rate window) allows us to determine the activation energy of the trap.

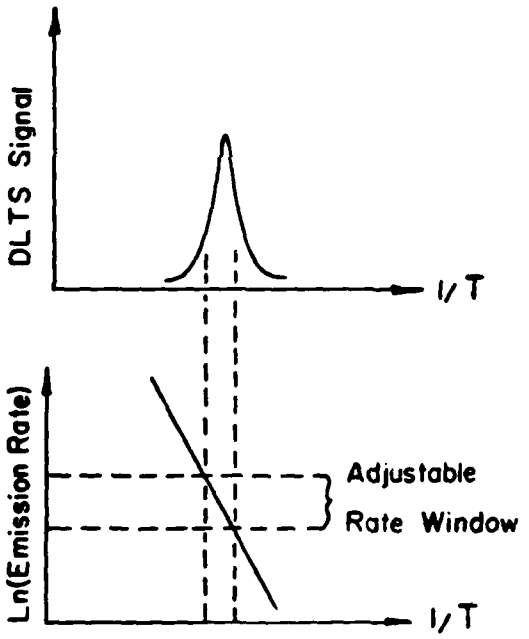

Fig. 5: Principle of the DLTS method: As the temperature is increased, the thermal emission rate for the trap increases. When it falls within the selected rate window, the system response shows a peak at that temperature.

In our experiment, we use a dual-gated averager (double boxcar) to set the emission rate window and to enhance the signal to noise ratio. The majority carrier pulse is repetitive and the capacitance transient is

sampled by the boxcar at t_1 and t_2 and the difference signal is averaged over many cycles to improve the signal to noise ratio. As the temperature of the diode is slowly increased, the time constant of the capacitance transient becomes shorter corresponding to the enhanced emission rate. A series of such capacitance transients at different temperatures is shown in Figure 6. The boxcar output $C(t_1) - C(t_2)$, called the DLTS signal, shows a peak at a temperature at which the emission

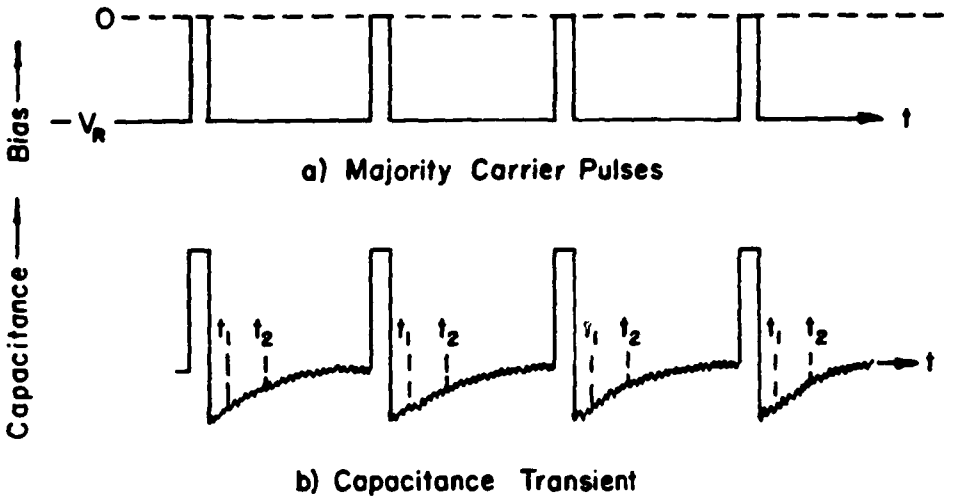

Fig. 6: Repetitive transients sampled and averaged at times t_1 and t_2.

rate falls in the rate window determined by t_1 and t_2.

It may be shown that the time constant τ of the transient capacitance at which the DLTS signal reaches a peak value is given by

$$\tau = \frac{(t_2 - t_1)}{\ln (t_2/t_1)} \qquad (9)$$

This principle is illustrated in Fig. 7.

A DLTS scan is made with the boxcar gates set at a particular set of values for t_1 and t_2 (generally keeping the ratio t_2/t_1 constant). A plot of $\ln (1/\tau)$ versus $1/kT$ gives the activation energy ΔE of the trap. We

can distinguish between majority carrier traps and minority carrier traps in DLTS scans. The majority carrier traps give negative DLTS peaks and vice versa.

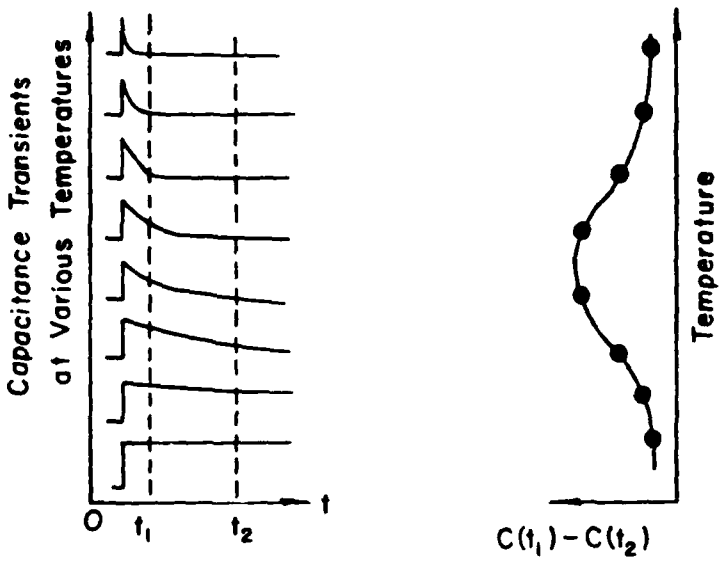

Fig. 7: Illustration of rate window defined by a double boxcar.

CHAPTER 2

2.1 Crystal Growth and Sample Preparation

The p-$Al_xGa_{1-x}As$ epitaxial layers used in this work were grown by the author at Stanford University using two different LPE growth systems -- a 'tilt' system and a 'slider' system. The crystals grown in the slider system were of much better quality in terms of surface morphology, smoothness of the interface, residual impurities, and heterojunction device characteristics. The doping levels were in the high $10^{16}cm^{-3}$ range and the deep level concentrations were low. The DLTS system at the Wright Patterson Air Force Base where the present experimental measurements were made was somewhat noisy, and it was not possible to obtain DLTS peaks using these relatively heavily doped samples. The p-$Al_xGa_{1-x}As$ epitaxial layers grown in the tilt system had lower carrier concentrations presumably because of compensation from residual impurities in the system. The surface morphology and the heterojunction device characteristics were poorer. However, the ratio of deep level concentration to the shallow acceptor concentration in these layers was high, and hence, it was possible to obtain large DLTS signals. Therefore, we shall briefly describe the tilt system used to grow the samples used in the DLTS experiments.

Figure 8 shows the schematic diagram of the tilt LPE growth system along with the fused quartz cradle and the graphite growth cell. A typical growth cycle was as follows. The system was flushed in purified hydrogen and the melt consisting of Ga, GaAs, Ge and Fe was baked out in the system for about 18 hours at 850 C in flowing hydrogen. The system was cooled to room temperature, the n+-GaAs:Te substrate was loaded in the substrate well, and aluminum was added to the melt. After again flushing the system

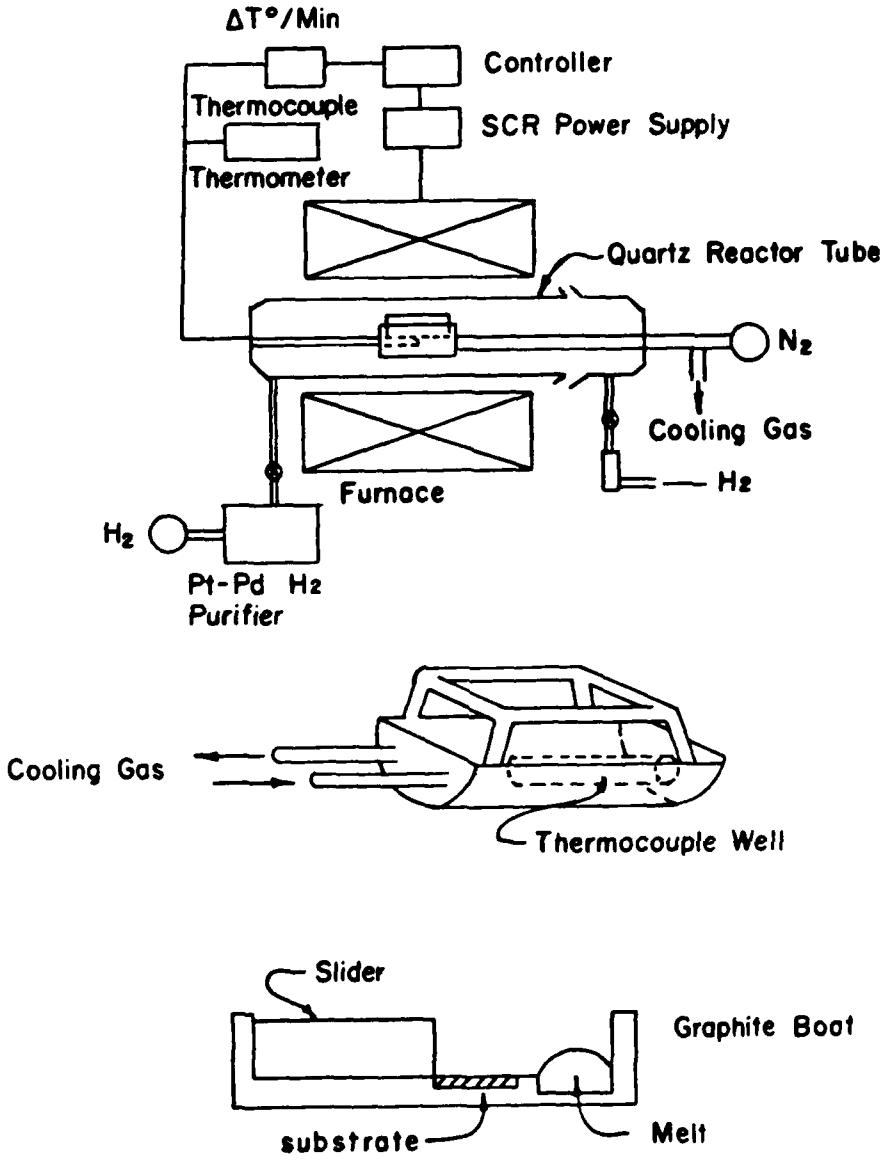

Fig. 8: LPE Growth System

in purified hydrogen for about half an hour at room temperature, the temperature was brought back up to 850 C. The furnace was tilted so that the melt was over the substrate and the epitaxial layer was grown by cooling the system at 1 C/min for 20 minutes. Then the furnace was tilted in the opposite direction so that the graphite slider could wipe the melt off the epitaxial layer and stop the growth. The system was then cooled to room temperature and the substrate was removed. The thickness of the grown epitaxial layer was measured by cleaving the wafer and staining it in PA solution (H_2O_2 + NH_4OH adjusted to a pH of 7.0). Typical layers were 2 to 4 microns thick. For samples with Al composition x<0.35, bandgap photoluminescence was measured at 77 K using a system consisting of a 4 watt Argon laser, a chopper, a 0.5 meter grating monochromator, a photomultiplier with an Sl response, and a lock-in-amplifier. To determine the value of x, it was assumed that at 300 K,

$$E_{g\Gamma}(x) = 1.424 + 1.142x + 0.504x^2 \qquad (10)$$

and where $E_{g\Gamma}(x)$ is the direct bandgap of $Al_xGa_{1-x}As$ corresponding to the Γ-valley of the conduction band at an aluminum composition x [6]. Further, the temperature dependence of $E_{g\Gamma}$ was assumed to be given by

$$E_{g\Gamma}(T) = E_{g\Gamma}(0) - \frac{5 \times 10^{-4} T^2}{T + 400} \qquad (11)$$

For layers with x>0.35, electron microprobe analysis was used to determine the aluminum composition. Au/Ge/Ni contacts were evaporated and alloyed at 450 C in flowing hydrogen to obtain ohmic contacts on the n+-GaAs:Te substrate and Au/Zn contacts were evaporated and alloyed on the p-$Al_xGa_{1-x}As$:Ge epitaxial layer. The diodes were cleaved to approximately 1mm x 1mm in size and mounted on TO-18 and TO-5 headers. I-V characteristics were measured to

determine the breakdown voltage and C-V characteristics were measured to determine the carrier concentration. The important characteristics of some of the diodes used in the DLTS measurements are given in Table I.

TABLE I

Diode Number	x	Thickness (microns)	Area (cm^2)	Breakdown Voltage (V)	Carrier Concentration (cm^{-3})
626x-2	0.39	2.4	7.9×10^{-2}	6	3.5×10^{16}
526x-2	0.56	3.5	1.7×10^{-2}	6	1×10^{15}
706x-1	0.71	2.4	1.8×10^{-2}	7	2.5×10^{16}

2.2 DLTS Measurements

A schematic of the DLTS experiment is shown in Figure 9. The DLTS system at the Wright-Patterson Air Force Base consisted of an Air Products Helitran refrigerator with a temperature controller which was capable of varying the diode temperature from about -30 K to +400 K, a Systron-Donner model 110B pulse generator with the capability of varying the dc bias from 0 to 10 volts, a Boonton model 72BD 1MHz capacitance meter with 2ms response

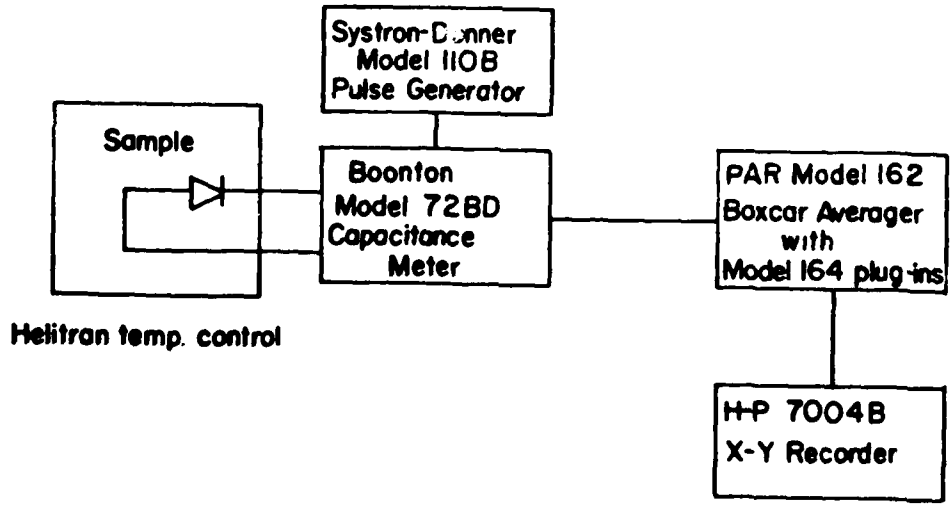

Fig. 9: Schematic of DLTS experiment

time, a Princeton Applied Research model 162 boxcar averager mainframe with two model 164 gated integrator plug-ins, and a Hewlett-Packard model 7004B x-y recorder. The p-$Al_xGa_{1-x}As$/n+-GaAs heterojunction diodes were mounted on TO-18 (and some on TO-5) headers. The thermocouple monitoring the junction temperature was attached to the metal can of the diode assembly. The output of the thermocouple was fed to the x-input of the x-y recorder through the Doric model DS-350 thermocouple indicator. The analog output of the capacitance meter was connected to the signal inputs of the two gated integrator plug-in modules. The A-B output of the model 162 boxcar averager was connected to the y-input of the recorder. A typical pulse width of 500 μs was used, and the majority carrier pulse was typically 1 to 4V in amplitude. The sampling gate width was typically 500 μs with a 100ms aperture delay range. The biasing pulse, the boxcar gates, and the transient capacitance were all monitored on a Tektronix model 5441 storage oscilloscope.

It was concluded that the thermocouple was not tracking the temperature of the diode with sufficient accuracy because of the location of the thermocouple with respect to the header by observing that the same DLTS peak occurred at slightly different temperatures while the sample was warming and cooling. Because of practical limitations and the lack of time, we were only able to minimize the tracking error to reasonable values (1 to 5 K) by warming and cooling at very low rates. Including the initial cooling down of the system, it was possible to get only two or three thermal scans per day. Figure 10 shows a typical capacitance transient signal observed on the monitoring oscilloscope. It represents the response from a hole trap in the p-$Al_xGa_{1-x}As$ layer.

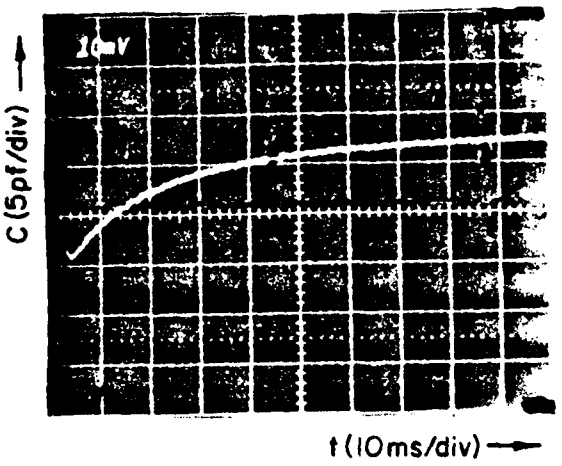

Fig. 10: Transient capacitance versus time for sample 706X-1 at 340 K

Figure 11 shows a DLTS thermal scan for sample 706x-1 in which the $Al_xGa_{1-x}As$ layer had an aluminum composition, x = 0.71.

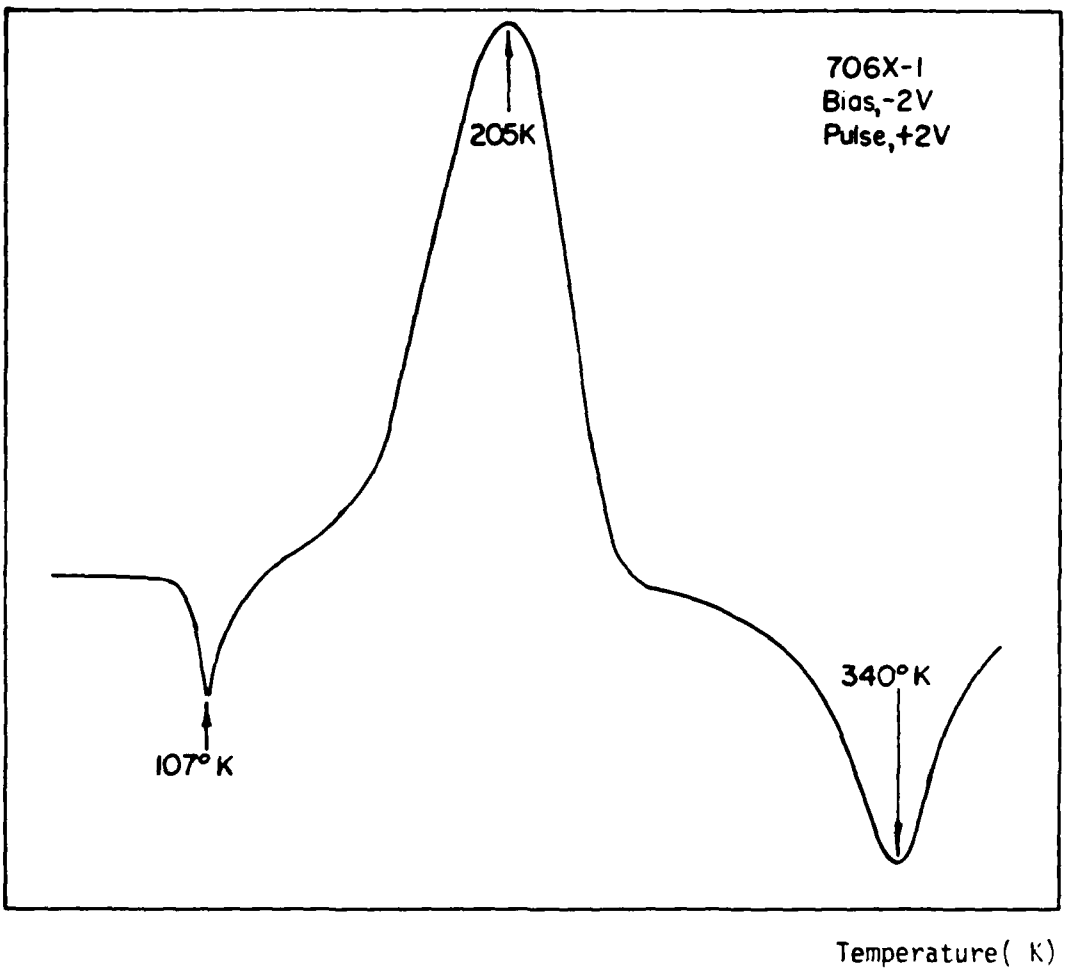

Fig. 11: A typical DLTS scan for sample 706X-1(X = 0.71)

We observe three DLTS peaks, two hole traps at 107 K and 340 K and an electron trap at 205 K. During the scan of the 205 K peak, the capacitance of the diode changed rapidly with temperature and a precision decade capacitor was used across the "DIFF" terminals of the capacitance meter

to avoid overloading of the boxcar input. The gate settings t_1 and t_2 which determine the rate window were changed over a wide range while keeping the ratio t_2/t_1 constant and a series of DLTS thermal scans were taken for diode 706x-1. Figure 12 shows the typical way in which a particular DLTS peak ("the high temperature peak") moves along the temperature axis as the rate window is changed. The emission rate window is determined by the gate settings t_1 and t_2 using

$$e = \frac{\ln t_2/t_1}{t_2 - t_1} \qquad (12)$$

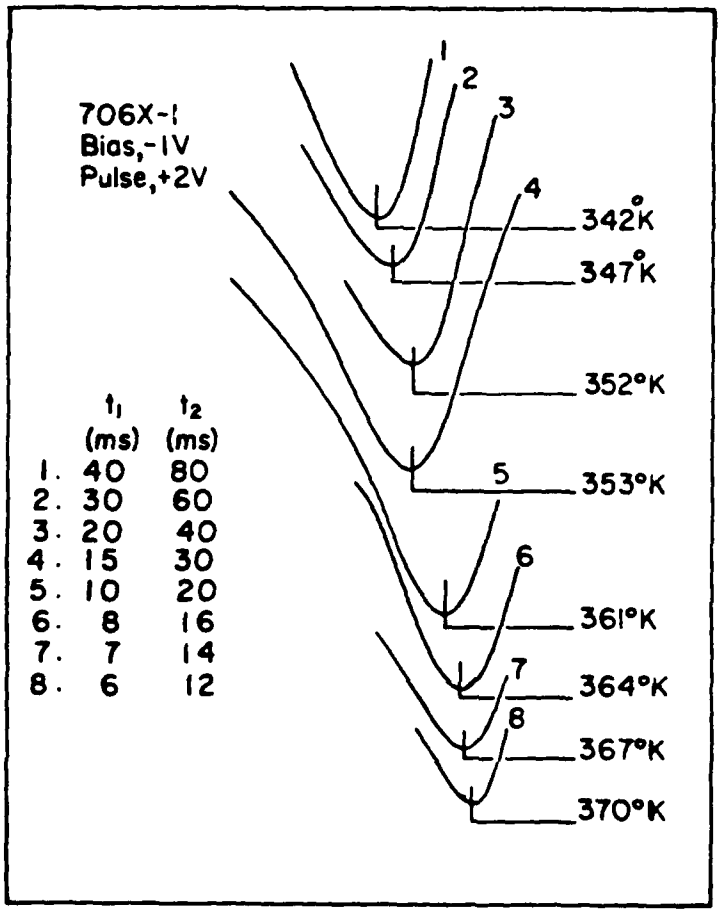

Fig. 12: Detailed measurements on the high temperature peak for sample 706X-1 (X = 0.71)

The DLTS peak moves from 342 K to 370 K for emission rate windows ranging from 17.3 sec^{-1} to 115.5 sec^{-1}. The emission rate of holes is given by

$$e_p = \frac{\sigma_p \langle v_p \rangle N_v}{g} \exp(-\Delta E/kT) \qquad (3)$$

If we use the temperature dependences of $\langle v_p \rangle$ and N_v from Eqs (4) and (5) and assume that the capture cross-section σ_p of the center for holes is not a function of temperature, we get

$$e_p = AT^2 \exp(-\Delta E/kT) \qquad (13)$$

Hence,

$$\ln(e_p/T^2) = \ln A - \Delta E/kT \qquad (14)$$

The plot of $\ln(e_p/T^2)$ versus $1/kT$ is a straight line with a slope, $-\Delta E$. Such Arrhenius plots for the DLTS peaks around 100 K, 200 K, and 340 K for the diode 706x-1 are shown in Figures 13, 14, and 15. The calculated activation energies are 0.27 eV, 0.35 eV, and 0.75 eV respectively. It should be noted that the 0.35 eV trap is an electron trap and is hence measured from the conduction edge while the other two are hole traps measured from the valence band edge. A year after this data was taken, the author visited the Wright-Patterson Air Force Base for a few days and was able to repeat some of the DLTS runs. This time, however, the activation energy of the electron trap was measured to be approximately 0.154 eV as seen in Figure 16. In an effort to check the DLTS data independently, the time constant, τ, of the capacitance transient was obtained by plotting the capacitance as a function of time

at several temperatures around 200 K. A plot of ln $(1/\tau T^2)$ versus 1/kT for this case is shown in Figure 17. The activation energy of the electron trap found in this manner was 0.165 eV. The earlier

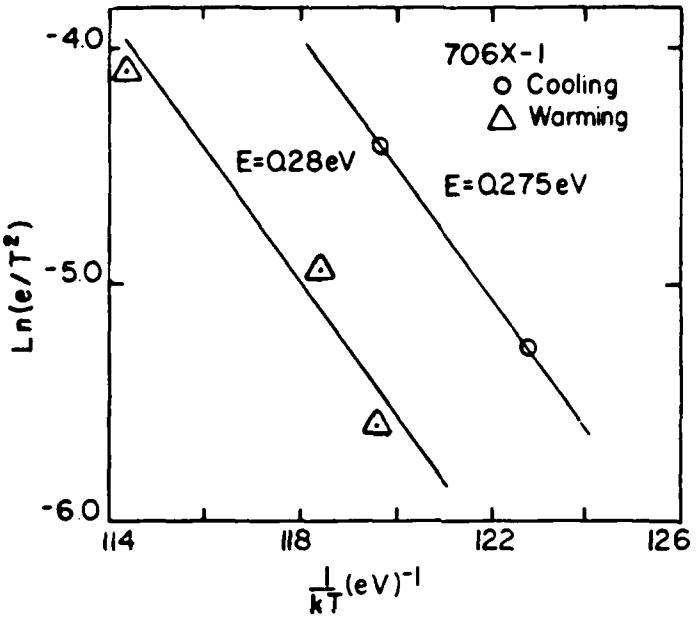

Fig. 13: Arrhenius plot of emission rate for sample 706X-1(V_R = -1 Volts, V_p = 1 Volts)

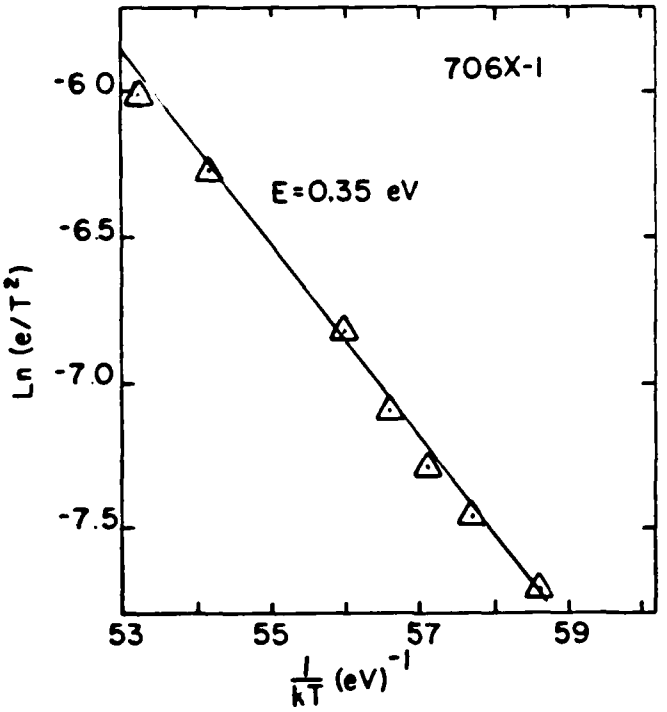

Fig. 14: Arrhenius plot of emission rate for sample 706X-1 (V_R = -4V, V_p = +4V)

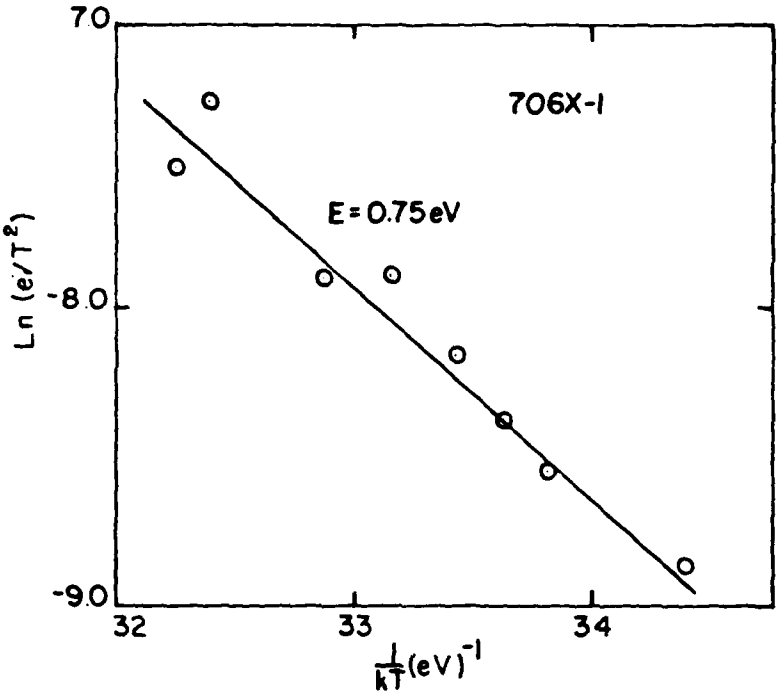

Fig. 15: Arrhenius plot of emission rate for sample 706X-1 (V_R = -2 Volts, V_p = +2 Volts)

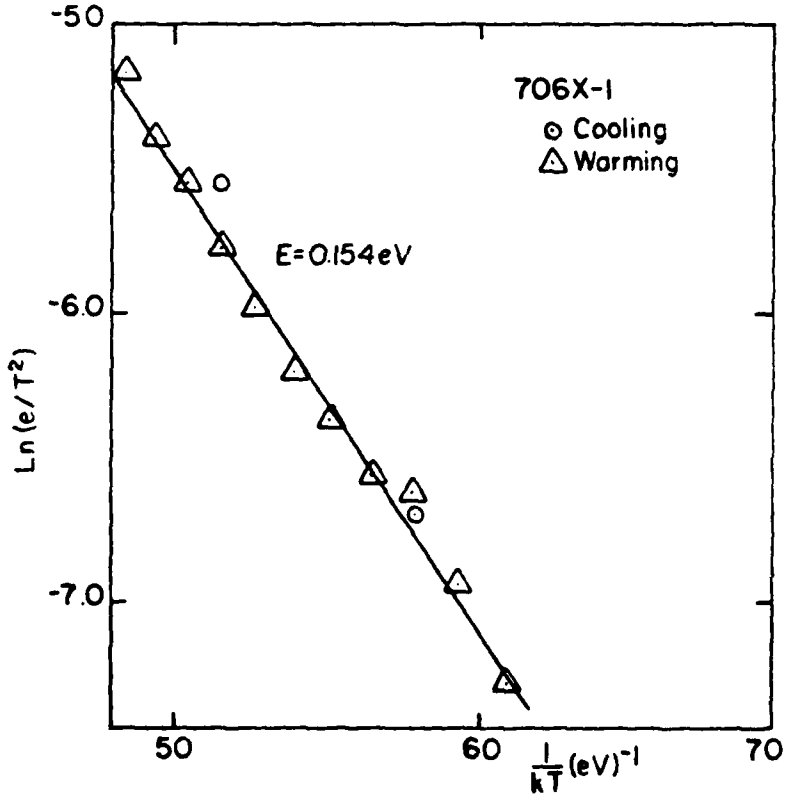

Fig. 16: Arrhenius plot of emission rate for sample 706X-1 (V_R = -4 Volts, V_p = +4 Volts)

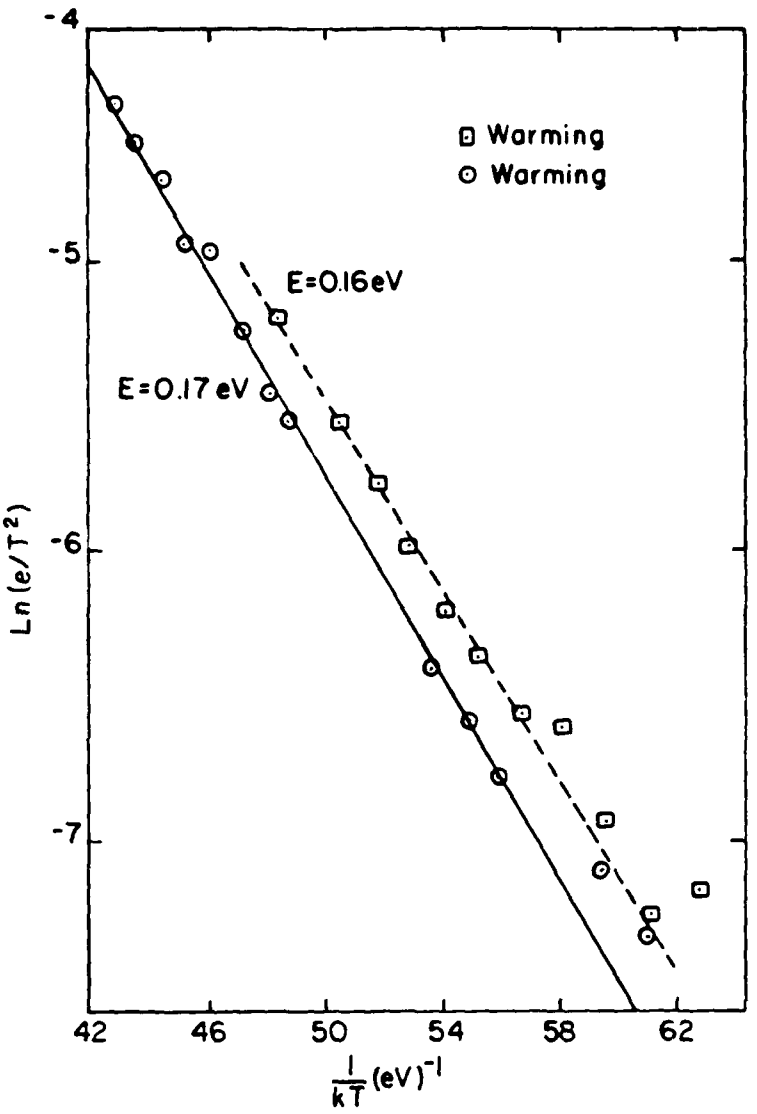

Fig. 17: Arrhenius plot of emission rate for sample 706X-1

data was taken using an injection pulse while the later data was obtained using a majority carrier pulse. It may also be noted that the DLTS peaks obtained while cooling the sample are shifted from those obtained while warming the sample because the thermocouple was not tracking the sample temperature well except at low warming and cooling rates. However, the slopes of the Arrhenius plots are approximately equal in the two cases.

For the diode 526x-2 with an aluminum composition, x = 0.56, we observed two DLTS peaks due to hole traps - a peak around 165 K with an activation energy of 0.49 eV and a peak around 340 K with an activation

energy of 0.46 eV. The Arrhenius plots are shown in Figures 18 and 19.

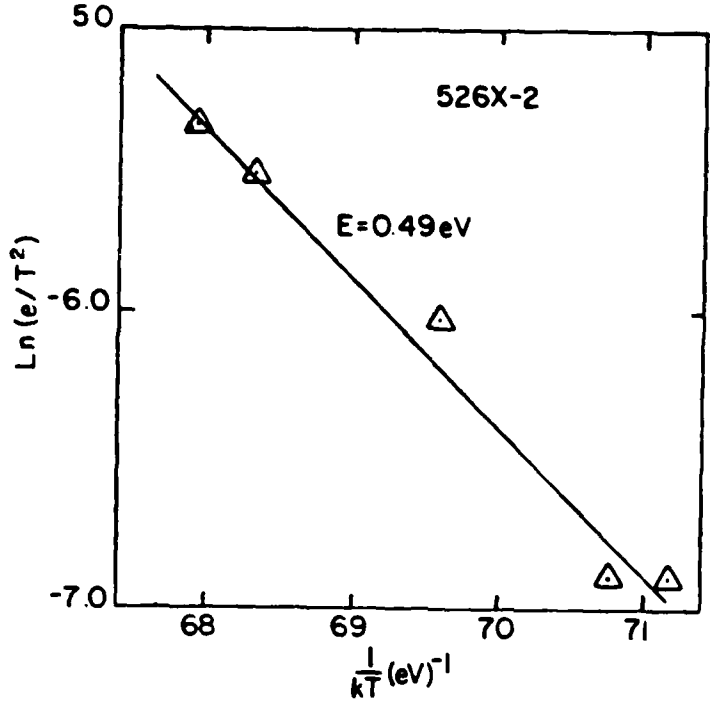

Fig. 18: Arrhenius plot of emission rate for sample 526X-2

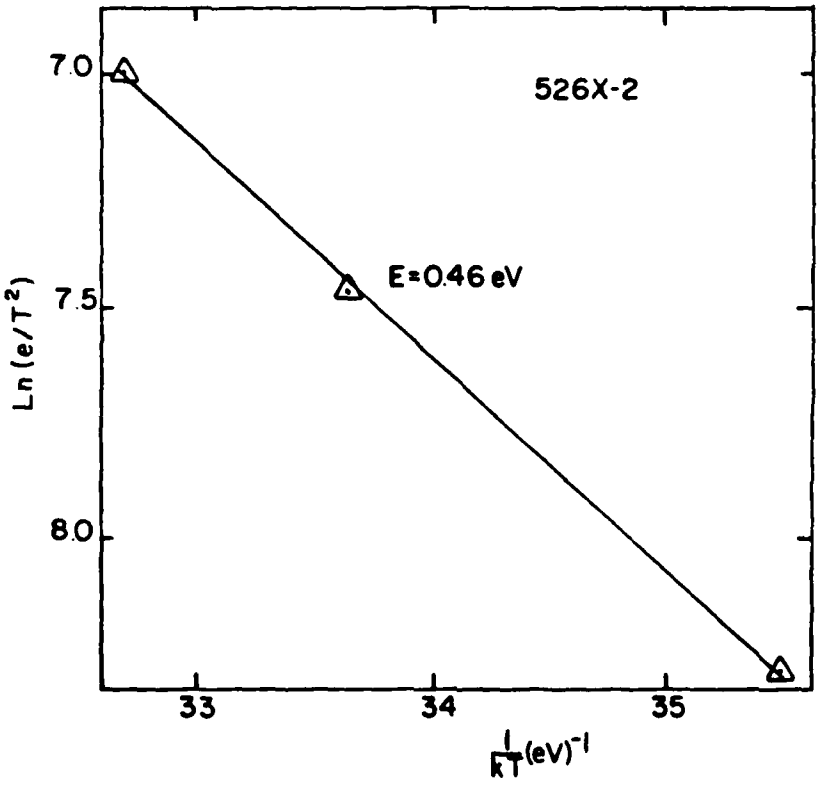

Fig. 19: Arrhenius plot of emission rate for sample 526X-2 (V_R = -2V, V_p = +2V)

For diode 626x-2 with an aluminum composition, x = 0.39, we observed four DLTS peaks around 45 K, 167 K, 285 K, and 395 K. As seen in Figure 20, these peaks are due to hole traps. The activation energies

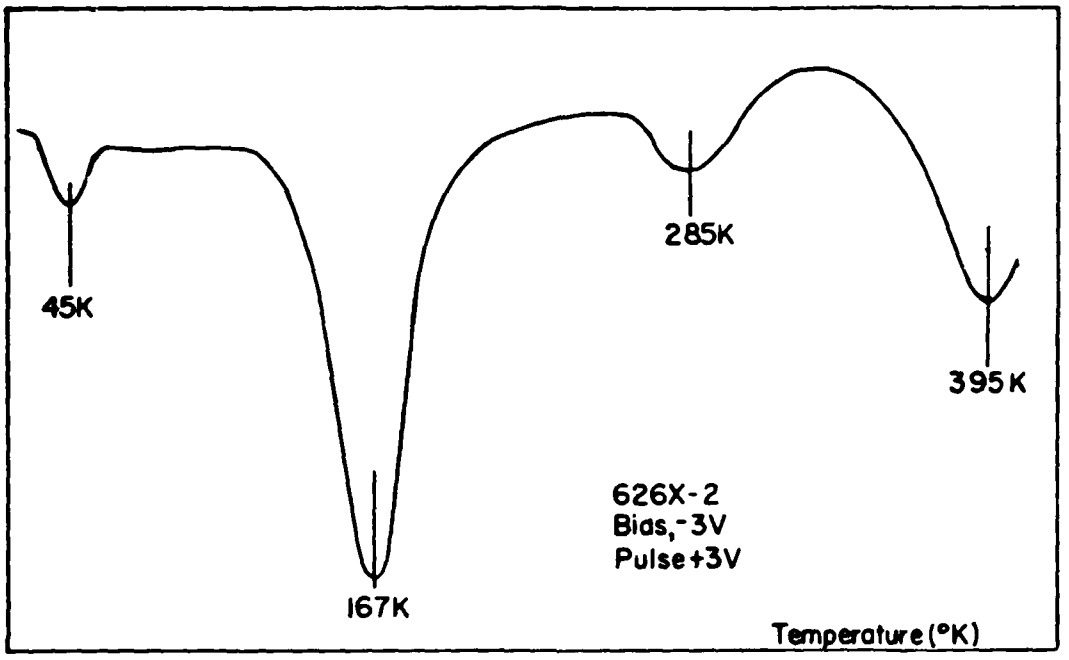

Fig. 20: A typical DLTS scan for sample 626X-2 (X = 0.39)

are approximately 0.012 eV, 0.22 eV, 0.48 eV, and 0.60 eV respectively. The Arrhenius plots for the 167 K peak for different values of the magnitude of the majority carrier pulse are shown in Figures 21 and 22. It is seen that the slopes of the Arrhenius plots are approximately equal for the data taken while cooling and heating the sample.

2.3. Calculation of the Deep level concentrations and the capture cross-sections of the traps.

When $\Delta C_0 << C_0$, and when the doping in the p-$Al_xGa_{1-x}As$ layer is spatially uniform, the trap concentration, N_T is given by

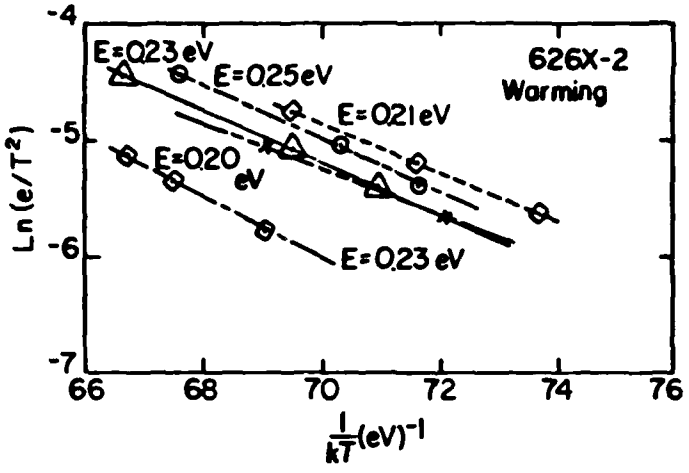

Fig. 21: Arrhenius plot of emission rate for sample 626X-2

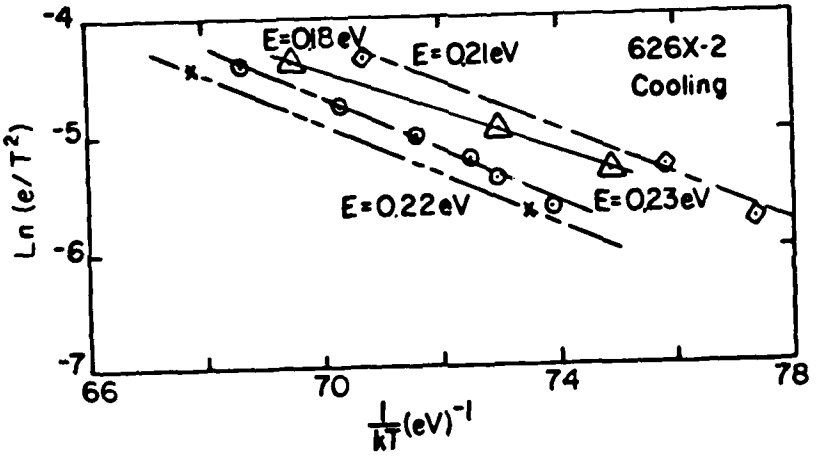

Fig. 22: Arrhenius plot of emission rate for sample 626X-2

$$N_T = 2\, N_A\, \Delta C_0 / C_0 \qquad (8)$$

where

N_A = net acceptor concentration in the depletion region on the p-side,

ΔC_0 = capacitance change due to completely filling a trap concentration N_T in the depletion layer,

C_0 = capacitance of the depletion layer under a fixed quiescent reverse bias.

The net acceptor concentration is obtained using the C-V plot for the heterojunction.

For the calculation of the capture cross-sections, we need m_h^* and m_e^*, the effective masses of the holes and the electrons in $Al_xGa_{1-x}As$. In the range $0.39 \leq x \leq 0.71$, we assume with Rheinlander et al [7] that

$$m_e^* \simeq 0.365\ m_0 \qquad (15)$$

In the same range, we assume with Casey and Panish [8] that

$$m_h^* = (0.48 + 0.31x)\ m_0 \qquad (16)$$

The experimental values of $\ln (e/T^2)$ may be used with Eqs. (3), (4), and (5) to solve for the capture cross-sections of electrons and holes for the various deep levels. The deep level concentrations and the capture cross-sections are shown in Table II.

Table II

ELECTRON AND HOLE TRAPS IN p-$Al_xGa_{1-x}As$ SINGLE CRYSTALS

Sample No.	Al Comp. x	Carrier Concentration N_A (cm^{-3})	Activation Energy E (eV)	Defect Density N_T (cm^{-3})	Capture Cross-section (cm^2)
626x-2	0.39	3.5×10^{16}	0.012	1.0×10^{15}	3.3×10^{-21}
			0.22	1.8×10^{15}	1.8×10^{-17}
			0.48	8.0×10^{14}	6.6×10^{-16}
			0.60	7.4×10^{14}	5.1×10^{-17}
			0.90	6.3×10^{14}	2.7×10^{-13}
526x-2	0.56	1.0×10^{15}	0.49	1.5×10^{14}	6.3×10^{-10}
			0.46	4.0×10^{13}	1.1×10^{-18}
706x-1	0.71	2.5×10^{16}	0.154**	2.0×10^{15}	5.4×10^{-21}
			0.35**	5×10^{15}	8.4×10^{-15}
			0.28	3.0×10^{15}	6.7×10^{-10}
			0.75	7.8×10^{14}	8.9×10^{-15}

** electron traps measured from the conduction band edge

The observed hole traps and their locations in the band gap are shown in Figure 23. The values of the band edges $E_{g\Gamma}$ and E_{gX} as functions of x are taken from Onton et al [6]. For comparison, the deep levels of Fe, Cu, and the so called 'A level' from Lang, Logan, and Kimmerling [9] are shown in the same Figure.

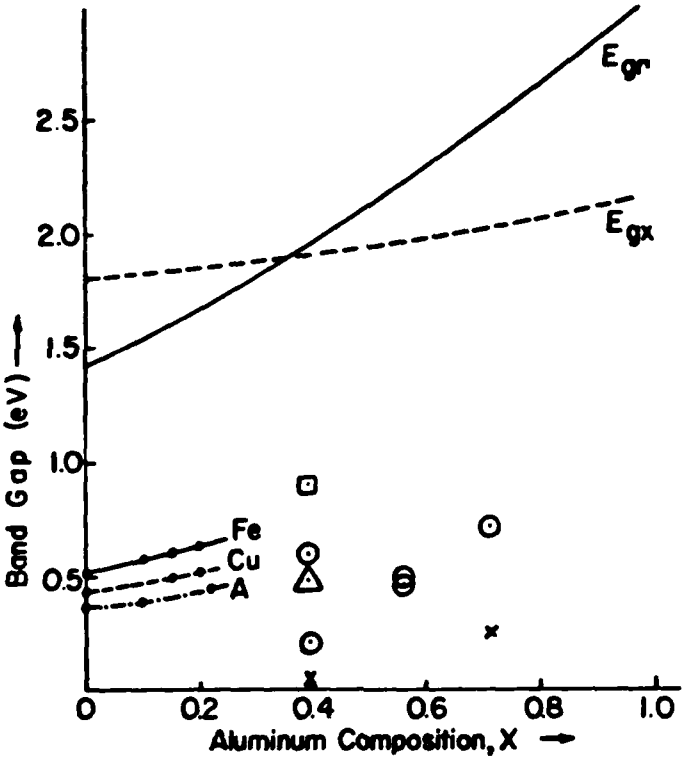

Fig. 23: Location of measured deep level in the bandgap as a function of aluminum composition.
⊙ ⊡ △- High temperature peaks, +x- Low temperature peaks

2.4 Photoluminescence measurements

Near band edge photoluminescence measurements on $Al_xGa_{1-x}As$:Fe single crystals were made using a photomultiplier detection system. A typical

spectrum is shown in Figure 24 for a sample with x = 0.25. Apart from the band edge photoluminescence at 0.69 μ there are two broad peaks around 0.85 μ and 1.01 μ. The deep level photoluminescence measurements were made using suitable filters and a cooled PbS detector. The samples 630A, 813B, 628, and 812A were grown on GaAs:Cr substrates and their photoluminescence spectra are shown in Figure 25.

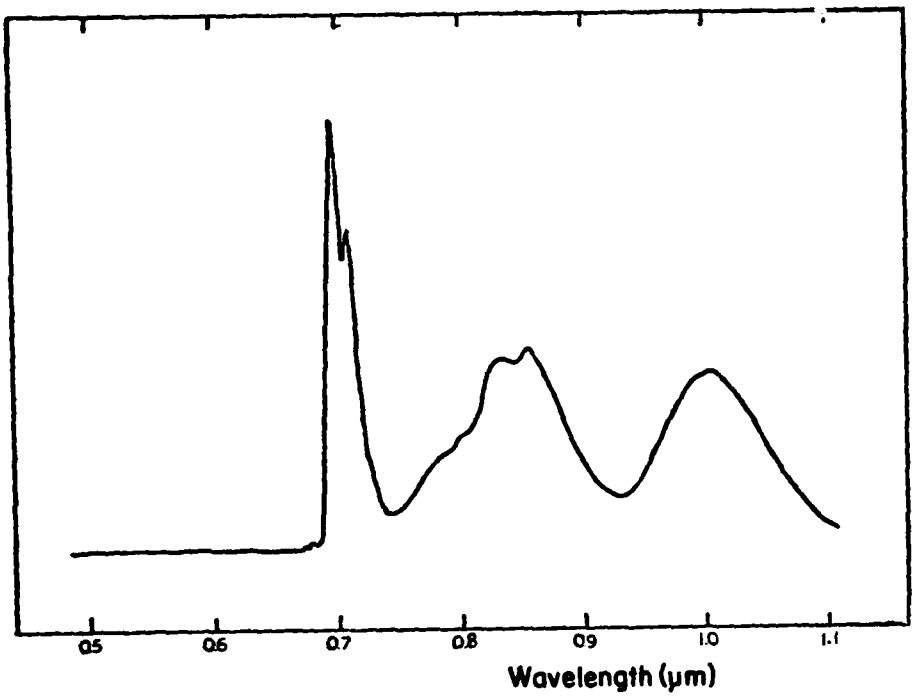

Fig. 24: Near band-edge photoluminescence measurements at liquid He temperature for sample 706B (x = 0.25)

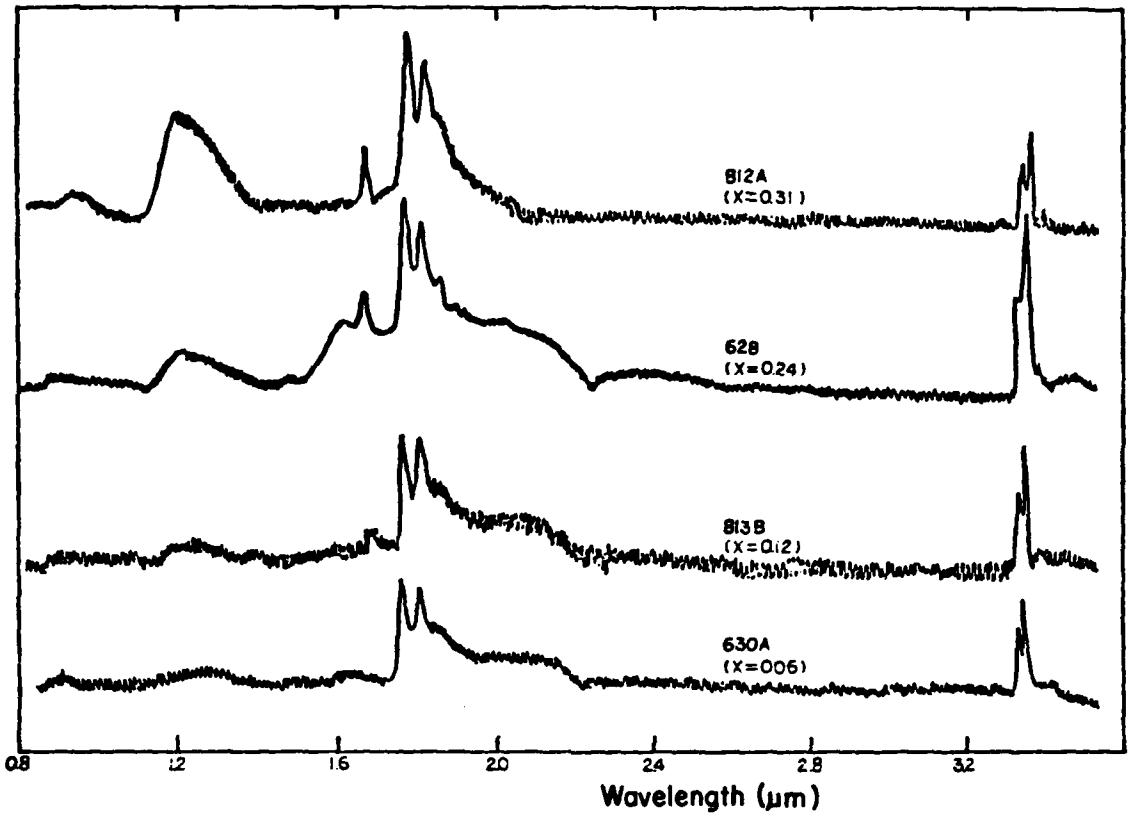

Fig. 25: Photoluminescence measurements at liquid He temperature using cooled -PbS detector

2.5 Conclusions and suggestions for future work

The observed hole traps at 0.48 eV and 0.6 eV in sample 626x-2, 0.46 eV and 0.49 eV in sample 526x-2 and 0.75 eV in sample 706x-1 appear to be related to the Cu acceptor levels or the so-called 'A levels' reported by Lang, Logan, and Kimmerling [9]. The 0.9 eV hole trap in the sample 626x-2 is probably due to Fe.

In the photoluminescence studies, the 1.23 eV peak corresponds to a hole trap consisting of a gallium vacancy bound to a Tellurium donor in GaAs reported by Hwang [10]. The sharp 0.37 eV peaks in the four $Al_xGa_{1-x}As$:Fe samples 630A, 813B, 628, and 812A correspond to the zero phonon line of Fe in GaAs. Koschel et al [11] ascribe it to an internal d-d transition from the $^5T_2$ excited state to the ^5E ground state of Fe^{2+} in GaAs. The lack of dependence of the peak energy with the aluminum composition may suggest that the optically excited carriers in the $Al_xGa_{1-x}As$ epitaxial layer diffuse into the GaAs substrate before recombining there. However, it is also possible that the emission is from the epitaxial layer. If the emission is due to an internal d-d transition between Fe^{2+} states, it is logical that the energy is independent of the aluminum composition as suggested by Kocot and Pearson [12] for the Cr peak in $Al_xGa_{1-x}As$:Cr.

The following suggestions are made for future work.

1. p/n^+ double layers of $Al_xGa_{1-x}As$ with x ranging from 0 to 0.5 and with acceptor concentrations in the p-layer ranging from 10^{15} cm^{-3} to 10^{16} cm^{-3} should be grown using a good slider system to obtain high quality layers with a high ratio of the intentionally added impurity (Fe) to the shallow acceptor concentration. Some layers with and some without Fe should be grown in otherwise identical conditions to enable us to identify the defects caused by Fe. The measured activation energies of

the deep levels may then be compared with the published data of Lang et al [9] for the range $0 \leq x \leq 0.2$. The diode geometries and their electrical characteristics may be improved by etching mesas. Furthermore, n/n^+ $Al_xGa_{1-x}As$ layers should be grown and Schottky barrier diodes fabricated in order to study the deep levels in n-type $Al_xGa_{1-x}As$. The DLTS system should be improved to obtain better tracking of the temperature by the thermocouple and to reduce noise and improve the sensitivity.

2. In the photoluminescence measurements, there is some doubt whether the 0.37 eV line is from the epitaxial layer or not. To settle this question, thick layers perhaps 100 μ thick may be grown on undoped GaAs substrates with low residual impurity concentration. A small area of the order of 2 to 3 mm in diameter of the substrate may be selectively etched off and the laser beam may be directed at the $Al_xGa_{1-x}As$ layer in this area. Under these conditions, most of the photogenerated carriers will recombine in the $Al_xGa_{1-x}As$ layer and the emission peaks will be due to defects in that layer.

REFERENCES

1. C.T. Sah, W.W. Chan, H.S. Fu, and J.W. Walker, Appl. Phys. Lett., 20, p. 193, 1 March 1972.

2. L.L. Rosier, and C.T. Sah, Solid-State Electron., 14, p. 41, 1971.

3. C.T. Sah, L.L. Rosier, and L. Forbes, J. Appl. Phys., 15, p.316, 1969.

4. L.D. Yau and C.T. Sah, Apol. Phys. lett., 21, p. 157, 1972.

5. D.V. Lang, J. Appl. Phys., 45, p. 3023, July 1974.

6. A. Onton, M.R. Lorenz, and J.M. Woodall, Bull. Am. Phys. Soc., 16, p. 371, 1971.

7. B. Rheinlander, H. Neumann, and M. Gropp, Leipzig, Experimentelle Technik der Physik XXIII, Heft 1, p. 33, 1975.

8. H.C. Casey, Jr. and M.B. Panish, Heterojunction Lasers, Part A, Fundamental Principles, Academic Press, New York, 1978.

9. D.V. Lang, R.A. Logan, and L.C. Kimmerling, Phys. Rev. B, 15, p. 4874, 15 May 1977.

10. C.J. Hwang, J. Appl. Phys., 40, p. 4584, 1969.

11. W.H. Koschel, U. Kaufmann, and S.G. Bishop, Solid State Commun., 21, p. 1069, 1977.

12. K. Kocot and G.L. Pearson, Solid State Commun., 25, p. 113, 1978.

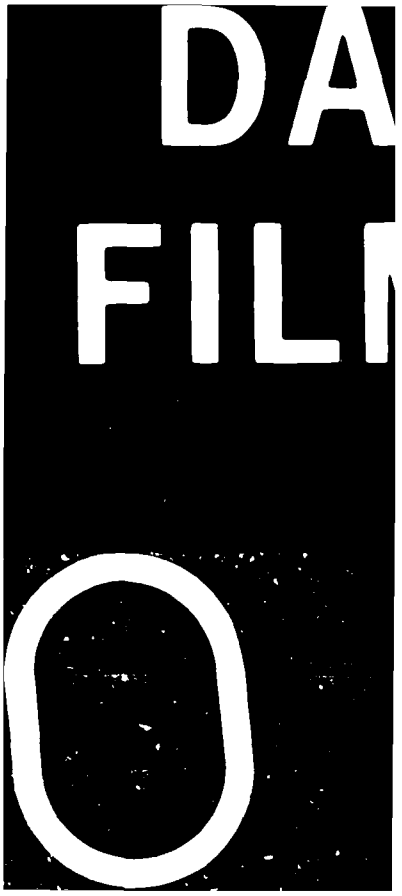
DA
FIL